The importance of accurate determination of optical constants for the design of nanometallic light-trapping structures

Phoebe Pearce[a,*], Alexander Mellor[a], Nicholas Ekins-Daukes[a,b]

[a]*Department of Physics, Imperial College London, South Kensington Campus, London, SW7 2AZ, UK*
[b]*School of Photovoltaic and Renewable Energy Engineering, UNSW, Sydney, NSW 2052, Australia*

Abstract

The optical constants of many metals commonly used in solar cells, e.g. as contacts, rear side planar reflectors, or more complex nanopatterned light-trapping structures, can vary depending on deposition method, thickness and other factors, and as such are not documented consistently in the literature. In the case of nanometallic light-trapping structures specifically designed to improve absorption in a solar cell, the choice of optical constants used in simulations significantly affects the predicted enhancement, as well as the structure's optimal dimensions. The trade-off between coupling into guided modes in the photovoltaic material and the number of photons absorbed parasitically in the metal leads to small differences in the optical constants giving significantly different results for the quantum efficiency and photogenerated current. This work documents several optical constant sources for silver, aluminium, gold and titanium, and the effect this has on plasmon quality factors. The effect of choosing different optical constant sources on modelling outcomes is quantified by considering the optimization of a test structure comprising a grid of metal nanodisks on the front surface of a thinned-down GaAs cell. Finally, we define a new spectrally-integrated figure of merit for comparing the expected performance of metals in light-trapping structures based on their optical constants, which we name the spectral absorption enhancement factor (SAEF).

Keywords:
Light-trapping, RCWA, Ultra-thin solar cells, Metallic gratings, Surface plasmons

1. Introduction

Arrays of metal nanoparticles [**?**], other diffracting structures using metal grids [**?**] or perforated films [**?**], and randomly arranged scattering nanoparticles [**? ?**] have all been investigated as methods for improving absorption in solar cells using plasmonic and diffraction effects [**? ? ?**]. Optical simulations are key in developing, analysing and optimising novel concepts for light-trapping architectures. In such structures, absorption in metal layers is parasitic, and thus in order to accurately predict solar cell performance (e.g. quantum efficiency and short-circuit current) it is critical to accurately quantify absorption in the target layer and in any parasitically absorbing layers.

A complicating factor in obtaining accurate simulation results is the uncertainty regarding the appropriate optical constants for commonly used metals such as gold, silver and titanium. The optical constants of nominally the same metal can vary depending on deposition process (e.g. bulk, evaporated, sputtered), sample thickness and other factors, leading different sources to report significantly different optical constants for the same material. These differences between sources may be exacerbated by instrumental error or the modelling approaches used to fit experimental data. Even metals grown by nominally similar methods can have different optical properties [**? ?**], and optical constant measurements may be affected by metal thickness and possible effects from surface layers; some metals will oxidise or tarnish if exposed to air, and interfaces between different materials may not be perfect. For instance, detrimental optical effects from a porous interface between silver and zinc oxide have been observed [**?**], and the incorporation of oxygen into aluminium nanodisks during growth affects their optical constants and plasmonic properties [**?**].

*Corresponding author.
Email address: phoebe.pearce15@imperial.ac.uk (Phoebe Pearce)

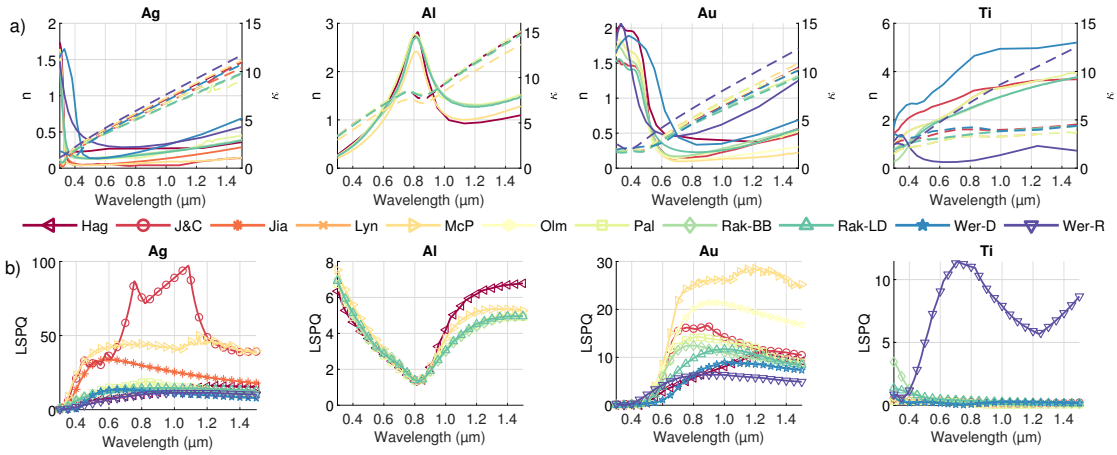

Figure 1: a) n (left axes, solid lines) and κ (right axes, dashed lines) for Ag, Al, Au and Ti, from different sources. Values were taken either directly from the published work (see Table 1) or from [**?**]. b) Localised surface plasmon quality factor, defined as $|n^2 - \kappa^2|/(2n\kappa)$ [**? ?**].

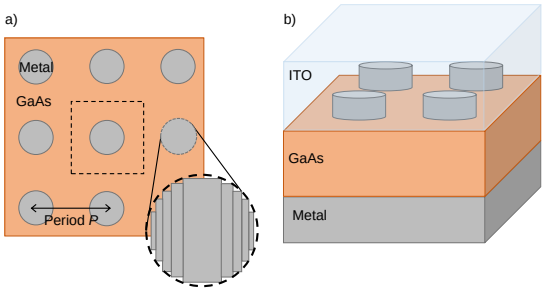

Figure 2: Schematic of the solar cell structure: a) Top-down view, with one unit cell outlined. The inset shows how the disks are built up in the RCWA method. b) Side view.

Table 1: Sources used for optical constant data, the labels by which they are referred to throughout this work, which of the metals considered here can be found in each reference, and a brief summary of the method by which the optical constants were measured or modelled.

Reference	Label	Metals	Method
Hagemann et al. [**?**]	Hag	Al, Ag, Au	Transmittance measurements of vacuum-evaporated films/Kramers-Kronig analysis
Jiang et al. [**?**]	Jia	Ag	Variable-angle spectroscopic ellipsometry of overlayer-protected films
Johnson & Christy [**?**]	J&C	Ag, Au, Ti	Reflection and transmission measurements on vacuum evaporated films
Lynch et al. [**?**]	Lyn	Ti	Absorptivity/reflectivity measurements of polycrystalline Ti/Kramers-Kronig analysis
McPeak et al. [**?**]	McP	Ag, Al, Au	Variable-angle spectroscopic ellipsometry of template-stripped samples
Olmon et al. [**?**]	Olm	Au*	Variable-angle spectroscopic ellipsometry of evaporated gold
Palik [**?**]	Pal	Ag, Al, Au, Ti	Various
Rakić et al. [**?**]	Rak-BB	Ag, Al, Au, Ti	Brendel-Bormann model fit to available experimental data
Rakić et al. [**?**]	Rak-LD	Ag, Al, Au, Ti	Lorentz-Drude model fit to available experimental data
Werner et al. [**?**]	Wer-R	Ag, Au, Ti	Reflection electron energy-loss spectroscopy (REELS)
Werner et al.[**?**]	Wer-D	Ag, Au, Ti	Density functional theory (DFT) calculations

There appears to be a bias towards the use of optical constants which give the most optimal results with little indication that these are the most appropriate data available; this was discussed in [**?**] for the case of silver optical constant data from Johnson & Christy [**?**]. This data has low extinction coefficient κ (and thus low absorption) and a high localized surface plasmon quality factor (LSPQ) compared to other data sources (see Fig. 1). Despite the availability of newer data and the large instrumental error reported in [**?**], this data continues to be used in recently published simulation results (e.g. [**? ? ? ? ?**]). Similar issues can readily be observed for other common metals including gold and titanium by comparing literature values of the optical constants.

In this work, four commonly-used metals are considered: silver, aluminium, gold, and titanium. In order to assess how the use of different optical constants affects simulation results, several different data sets from literature are used to optimize a simple solar cell-like optical structure in terms of optimal disk size and period of a regular scattering nanodisk array on top of a thin absorbing GaAs layer. In the cases of three of the four metals (all expect Al), variation in optical constants taken from different literature source in the wavelength region 300-900 nm lead to significantly different optimal arrangements for maximum absorption in the GaAs layer and thus photogenerated current (J_{ph}), and the predicted performance for these optimal structures also diverges. Differences in the J_{ph}, which depends on the number of photons absorbed in the GaAs, are not always reflected similarly in the total absorption; the total absorption profile may remain similar while the distribution of absorption between GaAs and metal layers changes significantly. Thus, care must be taken when comparing simulation results to total absorption measurements of optical precursor structures [**?** **?**], since accurate prediction of total absorption does not necessarily mean accurate prediction of absorption in the photovoltaic layer. Comparing the simulated J_{ph} results obtained for different metal sources with the newly-defined spectral absorption enhancement factor (SAEF) shows this new figure of merit to be a good predictor of the absorption enhancement performance of metals.

2. Methodology

2.1. Optical constant sources

Table 1 summarises the different sources used for the complex refractive index, $n + i\kappa$, of Ag, Al, Au and Ti, with references and the labels used to refer to each source throughout this work. Fig. 1a shows the refractive index n and extinction coefficient κ for each source. Not all sources have optical constant data for each of the metals considered here, and thus the number of data sets varies per metal (of course, more sources than those listed here are available). Although Palik's Handbook of Optical Constants [**?**] takes data from other sources, it is included here as a distinct source as it is very frequently cited and often the principal source when optical constant data is required. For each source, the localised surface plasmon quality factor (LSPQ) for a sphere[1] was calculated; this is defined in terms of

[1]The expression for LSPQ depends on nanoparticle shape; it is given here for a sphere, as this is a commonly-used figure of merit, although the nanoparticles simulated in this work are disks rather than spheres. The use of disks was due to the additional computational intensity required for modelling spheres using RCWA, as a sphere must be built from multiple layers in the vertical direction, as opposed to the single layer necessary for a disk/pillar.

the dielectric function $\epsilon_1 + i\epsilon_2$ as [**?** **?**]:

$$\text{LSPQ} = \frac{-\epsilon_1}{\epsilon_2} = \frac{|n^2 - \kappa^2|}{2n\kappa} \tag{1}$$

in the region where ϵ_1 is negative (i.e. metallic). The field enhancement in a material depends on ϵ_1, while the absorption (loss) depends on ϵ_2, and thus the LSPQ provides a convenient, easily-calculated figure of merit to estimate the potential for different metals in light-trapping structures.

2.2. Simulated structures

To quantify the light-trapping benefit from a metallic nanostructure, we consider a considerably thinned-down single-junction GaAs cell with a thickness of 50 nm (the thickness of the active layer of a thin-film GaAs cell is normally on the order of 2 μm); this is so that the light-trapping can, in theory, have a significant benefit since the GaAs is optically thin. The GaAs is covered by 60 nm of ITO, which acts as an anti-reflection coating (ARC) and encapsulates the metal nanoparticles (NPs). The metal NPs are disk-shaped pillars, and are arranged in a square grid as shown in Fig. 2. The same optical constants are used for the GaAs [**?**] and ITO [**?**] throughout all simulations, while those of the metal are from the sources specified. The cell has a metal back reflector made of the same metal as the NPs, which is considered to be a semi-infinite transmission medium in the simulations. The metal coverage fraction is defined as:

$$C = \frac{\text{area covered by metal}}{\text{total area}} = \frac{\pi r^2}{P^2} \tag{2}$$

when the cell is viewed as in Fig. 2a, where r is the nanodisk radius and P is the array period. Thus the maximum coverage fraction before the disks start to overlap is $\pi/4 = 0.79$, when $r = P/2$.

2.3. Simulation method

In the test structure, photons can be absorbed in the ITO/NP layer, the GaAs, or the metal back mirror. The normal-incidence absorptivity $A(\lambda)$ in each case is the fraction of incident power absorbed in that layer at a given wavelength λ. The spectrally weighted absorption Abs in each layer is then given by:

$$\begin{aligned} Abs_{NP} &= \frac{\int \Phi(\lambda) A_{NP}(\lambda) d\lambda}{\int \Phi(\lambda) d\lambda} \\ Abs_{GaAs} &= \frac{\int \Phi(\lambda) A_{GaAs}(\lambda) d\lambda}{\int \Phi(\lambda) d\lambda} \\ Abs_{back} &= \frac{\int \Phi(\lambda) A_{back}(\lambda) d\lambda}{\int \Phi(\lambda) d\lambda} \end{aligned} \tag{3}$$

Where Φ is the spectral photon flux for a standard AM1.5G reference spectrum [**?**]. The total spectrally weighted absorption Abs_{total} is given by $Abs_{total} = Abs_{NP} + Abs_{GaAs} + Abs_{back}$. The photogenerated current (J_{ph}) values, used as the primary indicator of performance for the simulated structures in the subsequent sections, were calculated using:

$$J_{ph} = q \int \Phi(\lambda) A_{GaAs}(\lambda) d\lambda \tag{4}$$

Where q is the elementary charge. Only absorption in the GaAs leads to photocurrent; absorption in the NP layer or back reflector are parasitic. Note that the term J_{ph} is used here since transport and surface recombination are not taken into account in these simulations. If an IQE of 100% is assumed, then J_{ph} is equal to the short-circuit current J_{SC}. Simulations and J_{ph} calculations were carried out over the wavelength range 300-900 nm, since spectral photon flux below 300 nm and interband absorption above 900 nm in GaAs (which has a bandgap of 875 nm) are negligible.

To calculate the fraction of photons absorbed in each layer at each wavelength, rigorous coupled-wave analysis (RCWA), sometimes referred to as the Fourier modal method (FMM), was used. RCWA is a method for solving

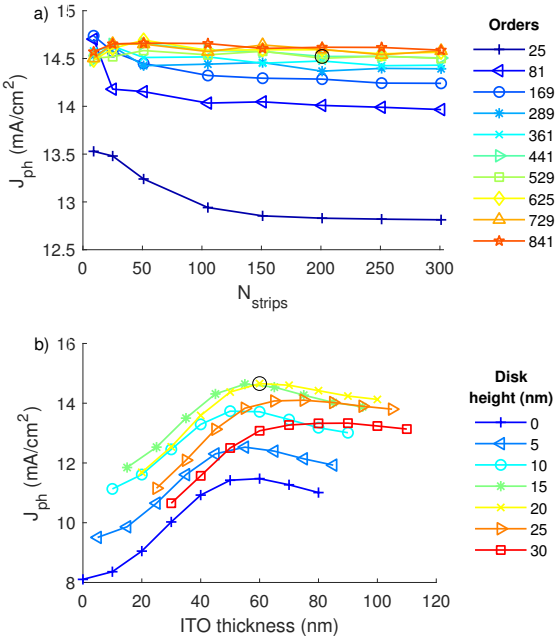

Figure 3: a) Calculated J_{ph} for a test structure as in Fig. 2 with nanodisk height 20 nm, ITO thickness 60 nm, GaAs thickness 50 nm, P = 500 nm and C = 0.5. The number of Fourier orders and strips to build up the disks (N_{strips}) is varied. The result for the number of orders and strips used to generate all the results in Section3 is circled in black. b) Calculated J_{ph} for the test structure with GaAs thickness 50 nm, P = 500 nm, C = 0.5 with different metal disk heights and ITO layer thicknesses. The result for the disk height and ITO thickness used to generate the results in Section 3 is circled. The metal optical constants used were those for silver from [**?**].

Maxwell's equations in periodic structures, and thus can be used to calculate diffraction and plasmonic effects due to metallic gratings. This is done by defining a structure which is periodic in two orthogonal lateral directions x and y. The electromagnetic field and permittivity at a particular height z perpendicular to the lateral directions can then be represented in terms of Fourier series, and a system of differential equations following from Maxwell's equations can be developed to solve for the field's Fourier coefficients as it propagates through the structure. Knowledge of the electric and magnetic field amplitudes in each diffraction order allows the absorbed and transmitted power to be calculated using the Poynting vector $\mathbf{S} = \mathbf{E} \times \mathbf{H}^*$. Specifically, calculating the z-component $\mathbf{S} \cdot \mathbf{z}$ at different heights in the structure allows changes in power flow across layers of interest to be calculated. The method requires that only a limited number of Fourier orders are retained in the calculation; a larger number of orders gives more accurate results, but leads to increased computation time. There are many implementations of RCWA available in different programming languages; GD-Calc (Grating Diffraction Calculator) [**?**], a MATLAB-based simulation tool, was used to calculate the results presented in this work. Since only rectangular blocks can be used, the nanodisks must be built up out of strips; the inset in Fig. 2a illustrates this using nine strips. Fig. 3a shows the convergence of the calculated J_{ph} with the number of Fourier orders and strips used for the circular disks for an example structure. The results in Section 3 were calculated using 441 Fourier orders and 201 strips. Considering calculations with a larger number of Fourier orders, the maximum deviation seen from the calculated J_{ph} value using these parameters was 1%, observed for 625 Fourier orders and 51 strips, indicating that the use of 441 orders and 201 strips was sufficient. Fig. 3a also shows that as long as a sufficient number of Fourier orders are used, the choice of the number of strips does not significantly affect the calculated J_{ph}.

2.4. Optimization

A simple grid search was performed covering the full parameter space of metal coverage C and array period P using each set of optical constant values, to produce a full map of the predicted J_{ph}, such as those in Fig. 4. With the resolution chosen, this meant around 300 simulations had to be performed in each case, and thus a High Performance Computing cluster was used. To reduce the parameter space, the height of the pillars (20 nm), ITO thickness (60 nm),

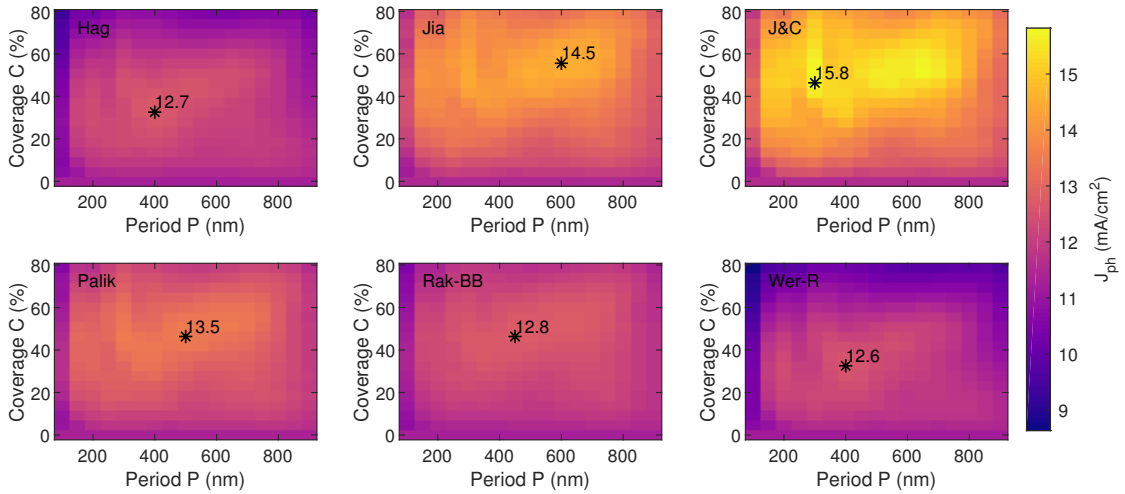

Figure 4: Predicted photogenerated current J_{ph} as a function of array period and metal coverage for the structure shown in Fig. 2 using six different sets of optical constant data for silver. The $*$ indicates the maximum J_{ph} (J_{max}), the value of which is labelled.

and GaAs thickness (50 nm) were kept constant, while the period of the array and metal coverage (i.e. radius of the disks) were varied. Fig. 3b shows an example of calculated J_{ph} with varying disk height and ITO thickness for a structure using silver [**?**], showing that a disk height of around 20 nm and total ITO thickness (including the ITO in between the metal disks) of around 60 nm are optimal. These optima will vary depending on the metal source and NP width/spacing, but were similar for several other arrangements and metals which were checked (with the exception of Ti, where generally the presence of any metal degrades the performance).

3. Results and discussion

3.1. Optical constants and figures of merit

Fig. 1 shows the optical constants and LSPQ for the different sources, grouped by metal. With the exception of Ti, the optical constants (Fig. 1a) for the same metal appear to follow the same trends, with apparently small deviations. However, these apparently small variations can lead to very large changes in the calculated LSPQ (Fig. 1b). The J&C data is a clear outlier for silver, and McP gives the highest LSPQ for gold, although the other sources also vary considerably. Unlike the other metals considered, the optical constants and LSPQ for aluminium were consistent across sources up to around 900 nm. For Ti, both the complex refractive index and thus, unsurprisingly, the LSPQ vary strongly depending on source, with the Wer-R data having an LSPQ more than 25 times higher than any other source around 0.7 µm. Overall, silver and gold have higher LSPQ than aluminium and titanium.

3.2. Predicted J_{ph} and spectral absorption

The metal coverage and array period giving the maximum J_{ph}, J_{max}, for each source are shown in Fig. 5, and detailed results on the optimum for each source are given in Table 2. In each case, the source with the highest peak LSPQ also gives the highest optimum J_{ph}. The spread of optimal solutions predicted using different sources is evident for all metals except Al, although there are also coinciding points for Ag, Au and Ti. For Ti, six out of seven sources predict that an NP array of the type considered here does not offer any potential for J_{ph} improvement, while Wer-R predicts a 15 % increase relative to the J_{ph} without NPs. To visualize the overall spread of results apart from the optima, Fig. 6 shows the results of all the simulations in terms of J_{ph} vs. metal coverage; for each source, the J_{ph} shows a clear trend, but these diverge significantly between sources for all metals except Al. Clearly, the choice of optical constant source has a significant effect when exploring possible arrangements for nanometallic structures in order to decide on an optimum for device fabrication.

Table 2 lists the optimal dimensions for nanodisk arrangement for each optical constant source. The overall optimum per metal is highlighted in bold. Table 3 shows the outcomes when this overall optimum arrangement is

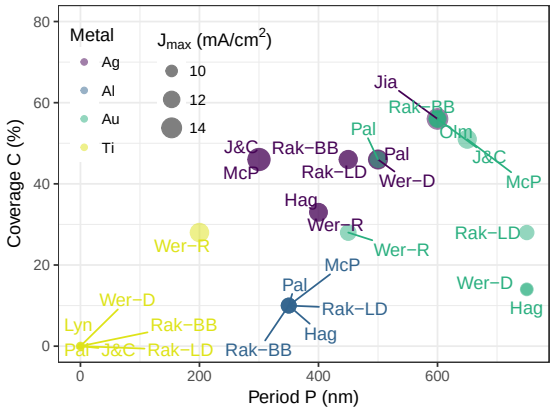

Figure 5: Location of the optimum configuration of nanodisks in terms of metal coverage and period for each optical constant source, corresponding to the points marked with $*$ for the illustrative cases in Fig. 4. The different colours indicate different metals, and the size of the point indicates the relative size of each maximum photogenerated current J_{max}. The point (0, 0) (i.e. 0 % metal coverage) means no nanoparticles are present, so the structure is bare GaAs with an ITO ARC and metal back mirror.

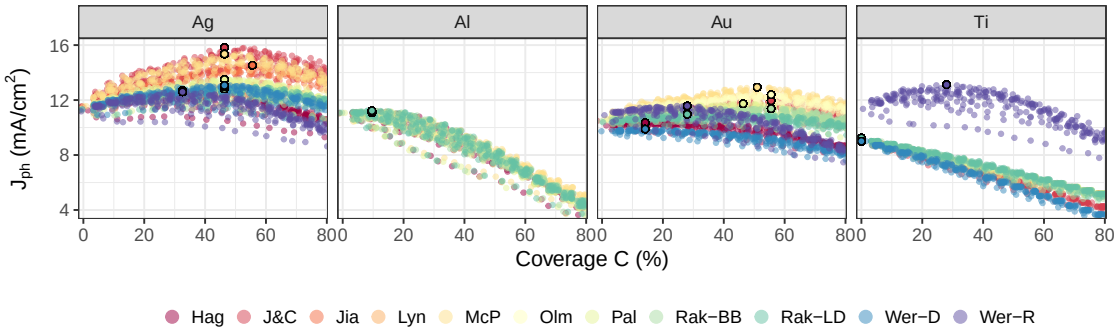

Figure 6: J_{ph} versus metal coverage C, showing the results of all the simulations (points are jittered slightly along the x-axis since C increases in discrete steps). Different colours represent different sources, and the point corresponding to J_{max} is outlined in black for each source (for Al, all these points coincide).

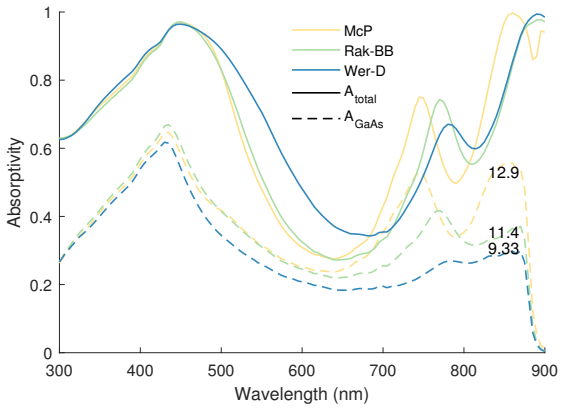

Figure 7: Absorptivity in the full structure (solid lines) and GaAs layer only (dashed lines) in the nanodisk structure with $C = 0.51$ and $P = 650$ nm using three different optical constant sources for Au. This is the arrangement which gives the overall maximum for gold when McP data is used. The labels indicate the predicted J_{ph} in mA/cm^2 due to absorption in the GaAs layer for each source.

Table 2: Detailed simulation results showing the J_{ph} without nanoparticles (J_0) and the optimal arrangement in terms of period P and metal coverage C leading to maximum photogenerated current J_{max}. The source giving the highest J_{max} is in bold for each metal. Also shown are the spectrally weighted absorption percentage Abs over the range 300-900 nm as defined in (3) for the whole structure (total), GaAs layer, ITO + nanoparticle layer (NP) and the back reflector. The spectral absorption enhancement factor (SAEF) calculated for each source according to (5) is shown in the final column.

Name	$\mathbf{J_0}$	$\mathbf{P_{opt}/C_{opt}}$	$\mathbf{J_{max}}$	**Spectral *Abs* (%)**				**SAEF**
				Total	**GaAs**	**NP**	**Back**	
Silver (Ag)								
Hag	11.3	400/0.33	12.7	58	41	9	7	208.09
Jia	11.5	600/0.56	14.5	57	45	9	3	802.81
J&C	**11.5**	**300/0.46**	**15.8**	**58**	**48**	**8**	**1**	**1144.1**
McP	11.6	300/0.46	15.4	58	47	9	2	1075.1
Pal	11.3	500/0.46	13.5	57	42	10	5	355.03
Rak-BB	11.3	450/0.46	12.8	57	41	10	5	303.35
Rak-LD	11.3	450/0.46	13.0	57	41	10	5	316.33
Wer-D	11.3	500/0.46	13.1	59	41	11	6	269.54
Wer-R	11.2	400/0.33	12.6	60	40	10	8	162.58
Aluminium (Al)								
Hag	11.0	350/0.10	11.2	62	38	6	18	111.42
McP	11.0	350/0.10	11.1	61	38	5	17	128.45
Pal	11.1	350/0.10	11.2	62	38	5	18	113.79
Rak-BB	11.1	350/0.10	11.2	62	38	5	18	118.26
Rak-LD	**11.1**	**350/0.10**	**11.2**	**62**	**38**	**5**	**18**	**118.97**
Gold (Au)								
Hag	10.1	750/0.14	10.4	56	35	5	16	61.913
J&C	10.5	600/0.56	12.0	63	37	16	10	178.1
McP	**10.6**	**650/0.51**	**12.9**	**63**	**39**	**14**	**9**	**249.49**
Olm	10.6	600/0.56	12.4	63	38	16	9	197.27
Pal	10.5	500/0.46	11.7	61	37	14	10	155.31
Rak-BB	10.4	600/0.56	11.4	62	35	16	11	143.73
Rak-LD	10.4	750/0.28	11.0	56	36	8	12	99.487
Wer-D	9.7	750/0.14	9.9	59	33	5	20	46.582
Wer-R	10.9	450/0.28	11.6	61	38	11	12	95.252
Titanium (Ti)								
J&C	9.1	0/0	9.1	73	32	1	39	11.176
Lyn	9.0	0/0	9.0	72	32	1	39	10.261
Pal	9.0	0/0	9.0	72	32	1	39	10.231
Rak-BB	9.2	0/0	9.2	69	33	1	36	29.741
Rak-LD	9.2	0/0	9.2	69	33	1	36	21.907
Wer-D	9.0	0/0	9.0	77	32	1	44	5.9927
Wer-R	**11.4**	**200/0.28**	**13.1**	**64**	**41**	**13**	**7**	**199.33**

Table 3: Best and worst outcomes, and the mean, using the nanodisk arrangements highlighted in Table 2 (i.e. those which give the highest overall J_{ph} in mA/cm^2 per metal out of all sources considered). Al is not included as there is no significant difference between sources.

Arrangement			**Best**		**Worst**		**Mean**
Ag	P = 300	J_{SC}	J&C	15.8	Wer-R	12.1	13.6
	C = 0.46	Abs_{total}		57.7		62.8	59.4
Au	P = 650	J_{SC}	McP	12.9	Wer-D	9.33	11.2
	C = 0.51	Abs_{total}		62.8		66.7	63.0
Ti	P = 200	J_{SC}	Wer-R	13.1	Wer-D	7.12	8.33
	C = 0.28	Abs_{total}		63.6		75.2	71.1

used to calculate the J_{ph} and Abs_{total} with the other optical constant sources for the same metal, reflecting a situation in which the structure is optimized using a specific set of optical constant data, which may not accurately predict behaviour in a manufactured optical structure or device. For Ag, Au and Ti, the percentage reductions between the best J_{ph} and the mean are 14%, 15% and 36%, respectively, indicating that unless the actual optical constants of materials used in a device match those used in simulations very closely, the solar cell performance may be significantly different to simulated predictions.

Tables 2 and 3 also compare the calculated J_{ph} with the total spectrally weighted absorption in the structure, Abs_{total}. The reader is reminded that only absorption in the GaAs produces photocurrent, whereas Abs_{total} considers all absorption in the structure, including in the ITO/NP layer and back reflector. Table 3 shows that while the J_{ph} predicted for identical NP arrangements using different optical constant sources varies considerably, the total absorption Abs_{total} (which includes contributions from the ITO/NP layer and back) over the range 300-900 nm does not necessarily vary similarly. In fact, for the cases shown in Table 3, Abs_{total} actually *increases* slightly between the best and worst-case sources for J_{ph}, due to increased parasitic absorption in the metal layers. The similarity of the absorptivity spectrum is shown for three different Au sources in Fig. 7, for the NP arrangement which gives the overall maximum for gold when McP data is used. Although the proportion of photons absorbed in the GaAs layer varies, the overall absorption spectrum shows similar peaks for McP, Rak-BB and Wer-D data. The variation in the spectrally weighted absorption Abs_{total} is also much smaller than corresponding changes in J_{ph}; this has important implications when comparing simulation results to e.g. total absorption measurements of optical precursor structures [**?** **?**]. While simulation results may match measured total absorption well, the absorption per layer and therefore J_{ph} in an optically equivalent device may differ greatly between simulation and experiment.

3.3. Case-study of impact on solar-cell modelling

As discussed in the introduction, many recently published simulation results continue to use silver data from J&C, which gives low parasitic absorption. An example is the multiresonant metallic nanogrid structure reported in [**?**]. This paper predicts a J_{ph} of 21.6 mA/cm^2 for an ultra-thin GaAs layer of 25 nm, using a biperiodic nanogrid of thickness 20 nm and period 500 nm (full details of the structure can be found in [**?**]). Fig. 8 shows calculated total absorption and absorption in the GaAs as reported in [**?**], and calculated using our RCWA implementation for three different optical constant sources. When using J&C data, the results both in terms of absorption profile and predicted J_{ph} (21 mA/cm^2) are very similar. However, using other sources significantly reduces the predicted J_{ph}. Jiang et al. [**?**] (labelled 'Jia' here) measured the optical constants of silver specifically to address the issue with the J&C data and provide new, realistic optical constants for evaporated silver; using these optical constants gives a J_{ph} 11 % lower than that predicted in [**?**]. Other sources give even worse outcomes, with Hagemann data giving a predicted a J_{ph} of only 14 mA/cm^2. All the data sources give similar resonant peaks to the J&C data in the total absorption spectrum, while the fraction absorbed in GaAs varies significantly. It should be noted that even the worst-case result shows impressive broadband absorption and a significantly enhanced J_{ph} compared to that of a similar structure without a metallic grating, which is around 10.5-11 mA/cm^2, depending on which optical constant data is used for the silver back reflector.

3.4. Origin of divergence

While the focus in this work is on investigating and quantifying the size of discrepancies between structures modelled using different optical constants, it is interesting to consider why the LSPQ, optimal arrangement of nanodisks, and predicted J_{ph} diverge, and how this is likely to impact the design of optical structures. In the case of Ti, the LSPQ for six out of seven sources considered is < 4 over the full wavelength range 300-900 nm, indicating that it is unlikely to perform well in the test structures, which is also the result obtained in the simulations for these six sources: the best option is not using any Ti NPs. Only one source is a significant outlier, giving much higher LSPQ, and this would be an unlikely choice for use in a simulation as it is a new result measured in an unusual way (reflection electron energy loss spectroscopy). However, even for the six sources which show Ti to be a poor material for these applications, the actual optical constants vary significantly, indicating that it is difficult to measure them accurately. The most obvious explanation for this is the presence of a (complex) surface layer which is not accounted for accurately when interpreting experimental data (e.g. a surface oxide or nitride). However, this does not explain why the data for Al is consistent when it is well-known that Al in air will form a stable aluminium oxide layer; it is likely that the oxidisation

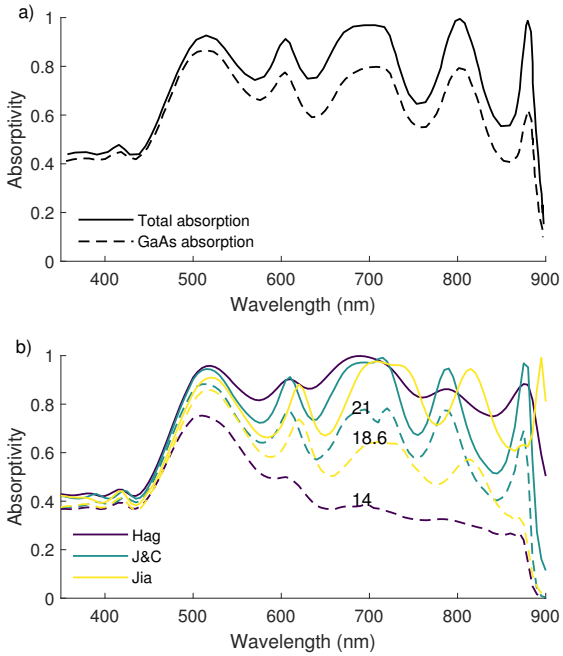

Figure 8: a) Calculated absorption in the total metal nanogrid + GaAs structure and in the GaAs layer only, as reported in [**?**]. b) Absorption for the same structure recalculated using our RCWA implementation for four different optical constant sources. The solid lines show total absorption while the dashed lines show absorption in the GaAs layer only. The labels indicate the predicted J_{ph} in mA/cm^2 due to absorption in the GaAs layer for each source.

behaviour of Ti is more complex, with oxygen penetrating into grain boundaries and forming TiO_2 rather than simply the formation of a self-limiting surface oxide layer as is the case for Al.

It appears that the J&C optical constants were impacted by silver tarnishing, as reported by Jiang et al. [**?**], who could replicate their results on unprotected silver with clear surface layer effects. As discussed in the introduction, the method and exact experimental parameters under which a metal is grown can affect its optical constants [**?**], meaning not all the divergence between sources is due to surface layers or experimental error, but rather due to inherent variation of behaviour for metals deposited under non-indentical circumstances.

3.5. Defining the Spectral Absorption Enhancement Factor of metals

In order to compare the maximum J_{ph} obtained for each optical constant source, J_{max}, with a single figure of merit, we define the spectral absorption enhancement factor (SAEF):

$$\begin{aligned} \text{SAEF} &= \int_{300\text{ nm}}^{\lambda_g} \text{LSPQ}(\lambda)\Phi(\lambda)d\lambda \\ &= \int_{300\text{ nm}}^{\lambda_g} \frac{-\epsilon_1(\lambda)}{\epsilon_2(\lambda)}\Phi(\lambda)d\lambda \end{aligned} \tag{5}$$

where λ_g is the wavelength corresponding to the bandgap of the absorbing semiconductor, set equal to 875 nm here for GaAs. By defining a new figure of merit in this way, the LSPQ at each wavelength is weighted by the solar photon flux at that point, i.e. the relative usefulness of increasing absorption at that specific wavelength. Fig. 9 shows the maximum photogenerated current J_{max} for optimised structures, as in Table 2, against the logarithm of the SAEF calculated from the data shown in Fig. 1b. There is a clear linear trend, showing that the SAEF is a useful quantity for comparing the expected absorption enhancement performance of a metal with a given set of optical constants without having to perform a large number of simulations to test different structures. It should be noted that SAEF as defined here depends not only on the metal, but also the absorbing semiconductor; the upper limit of integration is determined

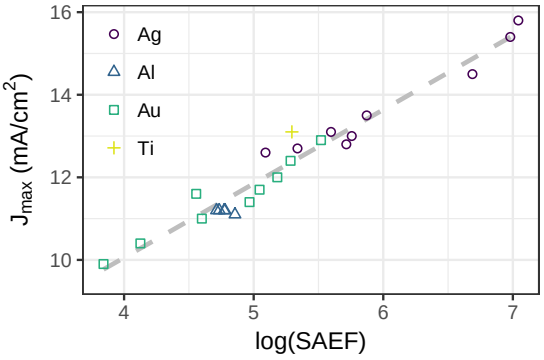

Figure 9: Maximum photogenerated current J_{max} obtained by optimising the test structure for each set of optical constant data (as in Table 2), plotted against the logarithm of the spectral absorption enhancement factor (SAEF), with the straight line of best fit. Only structures which actually include metal NPs are plotted, so six out of seven Ti structures are excluded as the J_{ph} was obtained by not including any metal.

by the bandgap of the absorbing material, as there is no utility in improving absorption at lower photon energies. The SAEF can be calculated straightforwardly from the optical constants of a metal and thus provides a much simpler method for predicting which materials will give the highest photocurrent enhancement.

When designing a solar cell structure, the SAEF could act as a useful guide in exploring different potential metals or optimising deposition conditions for a given metal, since it can be calculated directly from optical constants measured through e.g. variable-angle spectroscopic ellipsometry (VASE). Measuring the optical constants and thus calculating the SAEF for metal films grown under different deposition conditions would allow optimization of the process, or at least the selection of the best available process and/or metal. The metal with optical giving the highest SAEF, can then be used as input for simulations to find the optimal NP arrangement.

Further simulations are necessary to confirm whether the J_{ph} vs. SAEF trend holds for other NP arrangements and shapes, for different absorbers, or for metallic structures on the rear of the cell.

4. Conclusions

The effectiveness of periodic light-trapping structures containing metals is significantly affected by the exact optical constants of these metals, and thus obtaining realistic data for the specific application is key to matching experiment and simulation. Importantly, using inaccurate optical constants can lead to an incorrect optimal structure being identified. This provides a strong motivation for researchers to obtain optical constants of the metal films produced in their own facilities prior to designing a light-trapping structure. Where this is not possible, due caution must be take to use alternative data that corresponds well to the expected deposition conditions.

A new figure of merit, the SAEF, has been identified which predicts the suitability of a metal film for light-trapping applications. The SAEF can be determined directly from a metal's optical constants using a simple analytical expression, and has been found to correlate well with the photocurrent enhancement expected when that metal is used in an optimised light-trapping structure, as determined by rigorous simulations. This finding is useful for researchers and technologists, since it guides material choice, and allows deposition processes to be optimized without the need to repeatedly perform nano-fabrication and/or optical simulations for each deposition iteration.

Acknowledgements

The authors would like to thank the Imperial College High Performance Computing Service for the computational resources provided. PP would like to acknowledge EPSRC CASE sponsorship from IQE plc. AM would like to acknowledge the Engineering and Physical Science Research council (EPSRC) grant Joint UK-India Clean Energy Centre (JUICE) (EP/P003605/1). NED gratefully acknowledges a Royal Society Industry Fellowship.

References